Hindawi
Shock and Vibration
Volume 2019, Article ID 4389595, 13 pages
https://doi.org/10.1155/2019/4389595

Research Article

Hybrid Method of Modal Analysis and Laser Shock Scanning to Visualize the Pyroshock Propagation in a Tension Joint

Yong-Woon Kim,[1] **Jae-Kyeong Jang**,[1] **Jung-Ryul Lee**,[1] **and Hak-Seong Gim**[2]

[1]*Department of Aerospace Engineering, Korea Advanced Institute of Science and Technology, Daejeon, Republic of Korea*
[2]*The 4th R&D Institute, Agency for Defense Development, Daejeon 305-600, Republic of Korea*

Correspondence should be addressed to Jung-Ryul Lee; leejrr@kaist.ac.kr

Received 13 May 2019; Revised 4 July 2019; Accepted 24 July 2019; Published 27 August 2019

Academic Editor: Itzhak Green

Copyright © 2019 Yong-Woon Kim et al. This is an open access article distributed under the Creative Commons Attribution License, which permits unrestricted use, distribution, and reproduction in any medium, provided the original work is properly cited.

The use of pyrodevices in the aerospace industry has been increasing because of their ability to implement separation missions with a small weight, for example, space launchers, spacecrafts, and missiles. During operation, pyrodevices generate pyroshock, which causes failures of electronic devices. Recently, a pyroshock simulation method using laser shock has been developed to evaluate the risk of pyroshock before flight mission. However, depending on the structure, the laser shock showed some difficulty simulating pyroshock in the low-frequency regime accompanying vibration. Therefore, in this study, we developed a hybrid method of numerical modal analysis and laser shock-based experimental simulation to visualize the pyroshock propagation in all the relevant frequency regimes. For the proof of concept of the proposed method, we performed experiments of explosive bolt-induced shock and pyrolock-induced shock in the open-box-type tension joint and compared the hybrid simulation results with actual pyroshock. From the results, we obtained the simulated time-domain signal with an averaged peak-to-peak acceleration difference (PAD) of 11.2% and the shock response spectrum (SRS) with an averaged mean acceleration difference (MAD) of 28.5%. In addition, we were able to visualize the simulation results in the temporal and spectral domains to compare the pyroshock induced by each pyrodevice. A comparison of the simulations showed that the pyrolock had an impulse level of 1/12 compared to the explosion bolt. In particular, it was confirmed that the pyrolock-induced shock at the near field can cause damage to the electronic equipment despite a smaller impulse than that of the explosive bolt-induced shock. The hybrid method developed in this paper demonstrates that it is possible to simulate pyroshock for all the frequency regimes in complex specimens and to evaluate the risk in the time and frequency domain.

1. Introduction

Pyrodevices separate a substructure from a main structure via an explosion. Pyrodevices are widely used in the aerospace field because they have the advantages of enabling a separation mission with low weight and small volume [1, 2]. However, during operation, such a pyrodevice generates a high-frequency pyroshock, which causes failures in electronic devices [3]. According to a NASA technical memorandum published in 1988, 84 failures related with pyroshock occurred during 600 missile missions over 23 years, most of which were caused from the shock above 3 kHz [4]. Therefore, it is necessary to study the pyroshock to ensure the safety of the mission.

Pyroshock is divided into point-source pyroshock, linear-source pyroshock, and combined-source pyroshock, depending on the type of the pyrodevice. In addition, pyroshock is divided into three fields according to the magnitude and frequency of the response [5–7]. Figure 1 shows the pyroshock classification criteria. As shown in Figure 1, because the pyroshock includes broad-frequency band components, it is necessary to quantify the characteristics and risk of each. The most widely used quantification technique is the shock response spectrum (SRS), which is calculated based on the acceleration time history of pyroshock [8, 9].

Various simulation techniques have been developed to study pyroshock. Although there have been studies to

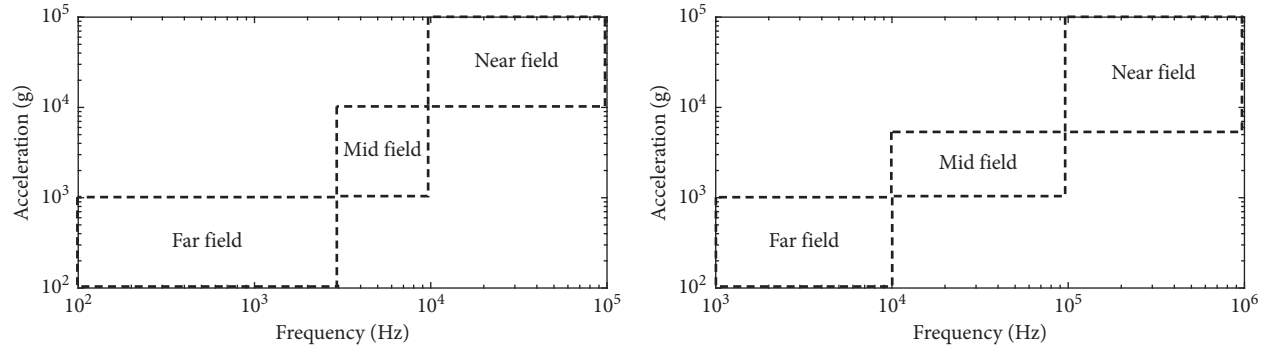

Figure 1: Pyroshock environmental categories: (a) IEST-RP-DTE032 and MIL-STD-810G [5, 6] and (b) NASA-STD-7003 [7].

simulate pyroshock using mechanical shocks, they all have limitations in that they can only be simulated for point-source pyroshock [10, 11]. In addition, finite element analysis has been used to simulate pyroshock in the low-frequency regime such as the far field. However, the finite element models used were not accurate for numerical simulation of the high-frequency structural response [12, 13]. Recently, research has involved simulation of pyroshock experimentally using laser shock. In this simulation approach, when the laser is irradiated onto the specimen, a thermal shock is generated via the thermoelastic mechanism, resulting in instant thermal expansion. These laser shocks contain a broad range of frequency components that were reported to be suitable for simulating pyroshock up to the high-frequency regime, such as those in the mid field and near field. In fact, various cases of pyroshock have been simulated using laser shock training based on an iterative signal decomposition and synthesis method [14]. However, this technique often showed low estimation accuracy in the low-frequency regime of subkilohertz frequencies, which might accompany engineering vibration, because the laser pulse-induced elastic wave contains primarily high-frequency components. In other words, laser shock-based simulation of the pyroshock accompanying subkilohertz vibration is very challenging to perform because of the structural boundary condition.

To overcome these limitations described above, we developed a hybrid method of modal analysis and laser shock scanning to simulate the pyroshock over the whole frequency regime. In the far field, with low-frequency components less than 3 kHz, because the finite element analysis verified the accurate simulation performance [12, 13], the far-field pyroshock was simulated using the modal analysis. In the mid and near field, because the laser shock-based experimental simulation provided accurate simulation performance [14], the mid- and near-field pyroshock over 3 kHz was simulated using laser shock. Each simulation result was superimposed and reconstructed to the pyroshock based on iterative signal decomposition and synthesis. In this study, the acceleration time history of pyroshock and the SRS are simulated. The simulation results are compared to actual pyroshock. A peak-to-peak acceleration difference (PAD) and a mean acceleration difference (MAD) are used to determine the similarity between the simulation results and the actual pyroshock. The PAD represents the error of the peak-to-peak response of the time-domain signal, and the MAD represents the error of the SRS between simulated results and the actual pyroshock [14]. There are other statistical measures which are commonly used to compare the similarity between signals such as correlation coefficient or root mean square deviation [15, 16]. However, in the pyroshock study, the similarity of the peak-to-peak acceleration is more important than the similarity of the whole signal in simulation of the time-domain signal.

The hybrid method developed in this study proves that the pyroshock can be simulated in a complex structure, such as an open-box-type tension joint; thus, the method can be used to evaluate the risk of pyroshock in the temporal and spectral domains.

2. Pyroshock Simulation Using the Hybrid Method of Modal Analysis and Laser Shock Scanning

Figure 2 shows the flow chart of the pyroshock simulation algorithm developed in this study. The algorithm is comprised of six steps. In the first step, actual pyroshock signals are measured using laser Doppler vibrometers (LDVs). In the second step, laser shock signals generated by a Q-switched laser are acquired through a broadband PZT sensor in a wave propagation imaging system (G-UPI, X-NDT Inc.). In the third step, modal analysis is performed on the subkilohertz vibration regime, often called the far field, even though the distance from the source is not far, and then the result is superimposed on the laser scanning data and stored as reference data. In the fourth step, the difference between the reference data and the actual pyroshock is analyzed based on the SRS, and then, the optimized gain value for correcting the difference between the two signals is selected and applied to predict the SRS of pyroshock. In the fifth step, the information of the predicted SRS is given to the laser scanning data using an iterative signal decomposition and synthesis method developed in [14] to simulate the time-domain signal of the pyroshock at all the scan areas. In the final step, the pyroshock wave propagation image (PWPI)

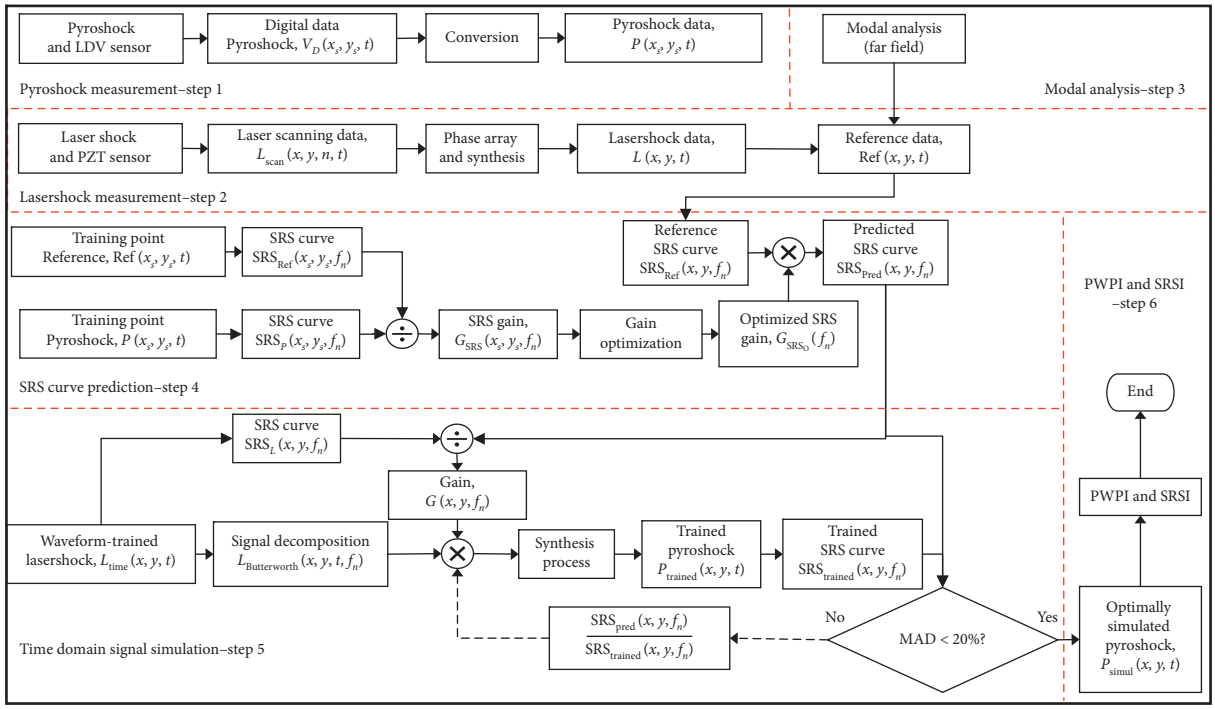

FIGURE 2: Flow chart of the hybrid method of FEM-based modal analysis and laser shock scanning-based simulation (PWPI: pyroshock wave propagation imaging; SRSI: shock response spectral imaging).

and the shock response spectrum image (SRSI) are obtained using simulated pyroshock signals and spectra, respectively.

2.1. Pyroshock Measurement on an Open-Box-Type Tension Joint. A 1/2-inch explosive bolt (Hanwha Corporation), shown in Figure 3(a), is a conventional pyrodevice, which is separated by a ridge-cut mechanism [17]. The explosive bolts have advantages of simple operation and low weight, but they have the disadvantage of providing a large impulse. Figure 3(b) is a pyrolock device (Hanwha Corporation) designed to reduce the impulse of the explosive bolts. In this study, we used the developed hybrid method to simulate the explosive bolt-induced shock and the pyrolock-induced shock and then compared them in time and frequency domains. In the experiment, an open-box-type tension joint made of a stainless-steel material was used to simulate the environment in which the substructure is separated from the main structure. The open-box-tension joint has four surfaces with one free edge where considerable vibration is also induced via explosion. Two types of pyrodevices were installed on the specimens, and pyroshock signals were measured using three LDVs. Details of the measurement point and test specimens are shown in Figure 3(c). The coordinates of the measurement points are represented by (x_s, y_s). The voltage signals collected from the LDVs are stored in the PC, where the pyroshock voltage signal is denoted by $V_D(x_s, y_s, t)$. $V_D(x_s, y_s, t)$ is then converted to the pyroshock signal, $P(x_s, y_s, t)$, of the acceleration unit through a conversion process using equation (1). The detailed conditions of data acquisition are listed in Table 1:

$$P(x_s, y_s, t) = \left[\frac{d\left(V_D(x_s, y_s, t) \times \mathrm{CF} \times 10^{A_{\mathrm{dB}}/20} \times \mathrm{CF}_{\mathrm{mr}}\right)}{dt}\right], \tag{1}$$

where $V_D(x_s, y_s, t)$ is the pyroshock signal of digital voltage form (V), $P(x_s, y_s, t)$ is the pyroshock signal of the acceleration unit (g), CF is the calibration factor of LDV, A_{dB} is the attenuation factor of the attenuator, and $\mathrm{CF}_{\mathrm{mr}}$ is the measurement unit of the LDV sensor (m/s/V).

2.2. Laser Shock Scanning Measurement on the Open-Box-Type Tension Joint. Through the pyroshock measurement process, we can observe the characteristics of the pyroshock. However, the point measurement of the actual pyroshock at limited points is not sufficient to understand and analyze the pyroshock that is propagated over the structure. To visualize the propagation of pyroshock in the full field over the structure, we simulate pyroshock using laser shock. The same structure used in the pyroshock measurement was prepared to obtain the laser shock signals. Next, PZT sensors were installed in place of the pyrodevice, as shown in Figure 4, because the reciprocal setup of the laser shock scanning system with a wavelength of 532 nm (G-UPI, X-NDT Inc.) designates the sensor locations' shock source locations. Subsequently, the laser scanning process was performed by setting the signal acquisition conditions through the GUI platform. The laser shocks generated by using the Q-switched laser were collected through a PZT sensor, and the obtained laser scanning data were represented by $L(x, y, t)$, depending on the laser shock location. In this case, the scanning area was set to include pyroshock measurement points, as shown in

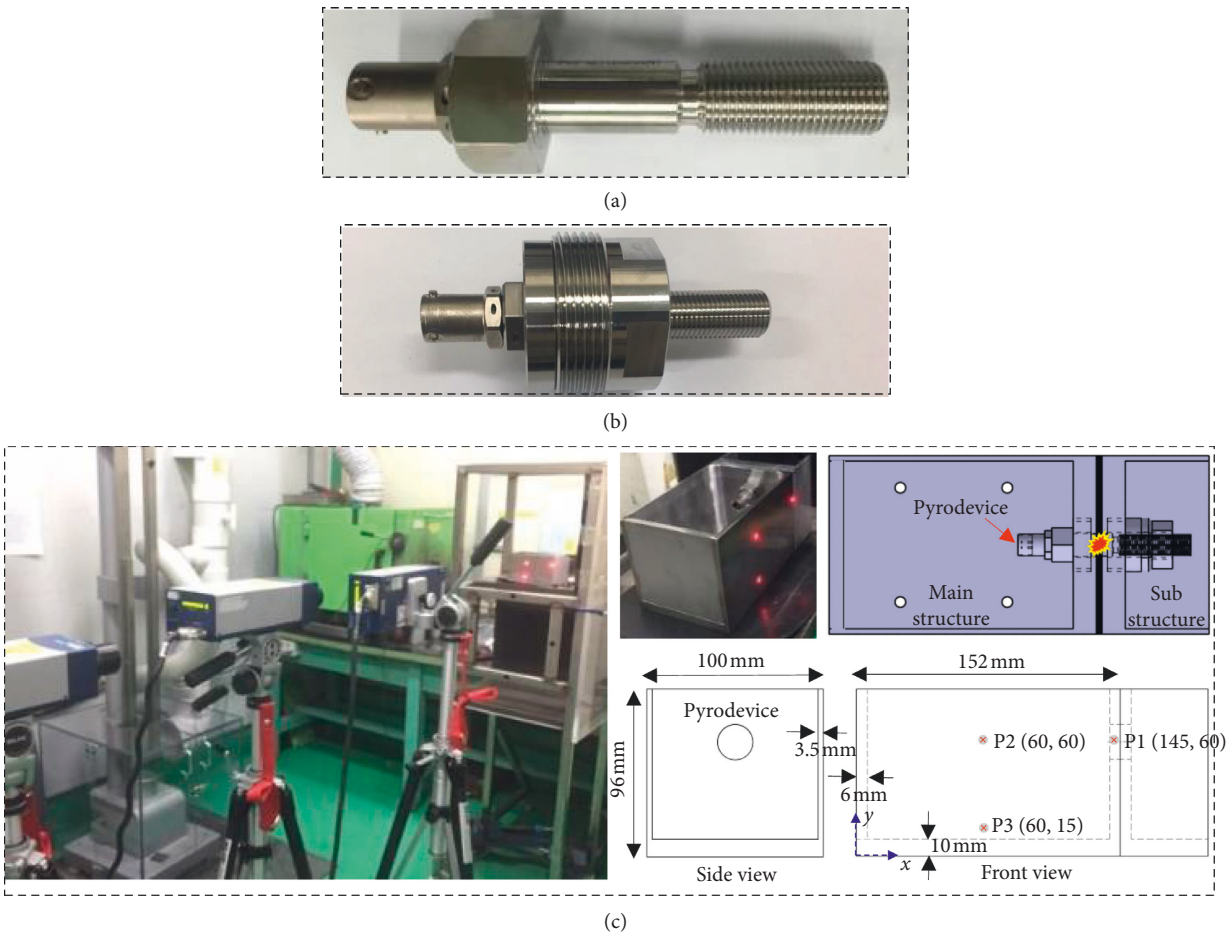

Figure 3: (a) 1/2-inch explosive bolt, (b) 1/2-inch pyrolock, and (c) measurement setup of pyroshock on the open-box-type tension joint.

Table 1: Data acquisition condition of pyroshock on the open-box-type tension joint.

Shock source	CF	F_s (MHz)	Filter (kHz)	Number of samples	CF_{mr} (mm/s/V)	A_{dB} (dB)	Sensing point coordinate
Pyroshock	$CF_1 = 1.42$	1	0.1~100	30,000	1,000	$A_{dB1} = 9$	Point 1–(145, 60)
	$CF_2 = 1.42$					$A_{dB2} = 6$	Point 2–(60, 60)
	$CF_3 = 1.42$					$A_{dB3} = 6$	Point 3–(60, 15)

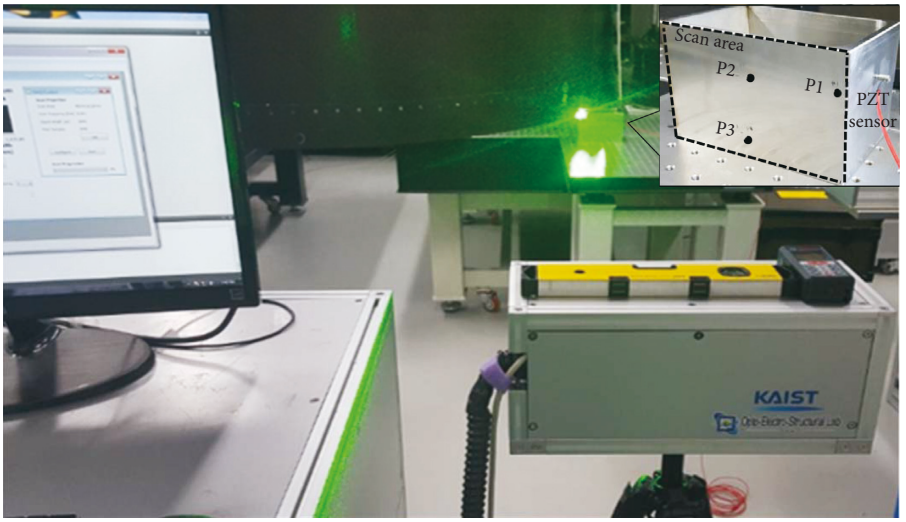

Figure 4: Laser scanning measurement setup for simulation of pyroshock on the open-box-type tension joint.

Table 2: Measurement conditions of laser scanning for simulation of pyroshock on the open-box-type tension joint.

Shock source	F_s (MHz)	Filter (kHz)	Number of samples	PRF (Hz)	Scan area (mm)
Laser shock	1	0.1~100	8,000	50	Width = 152 Height = 96 Interval = 1

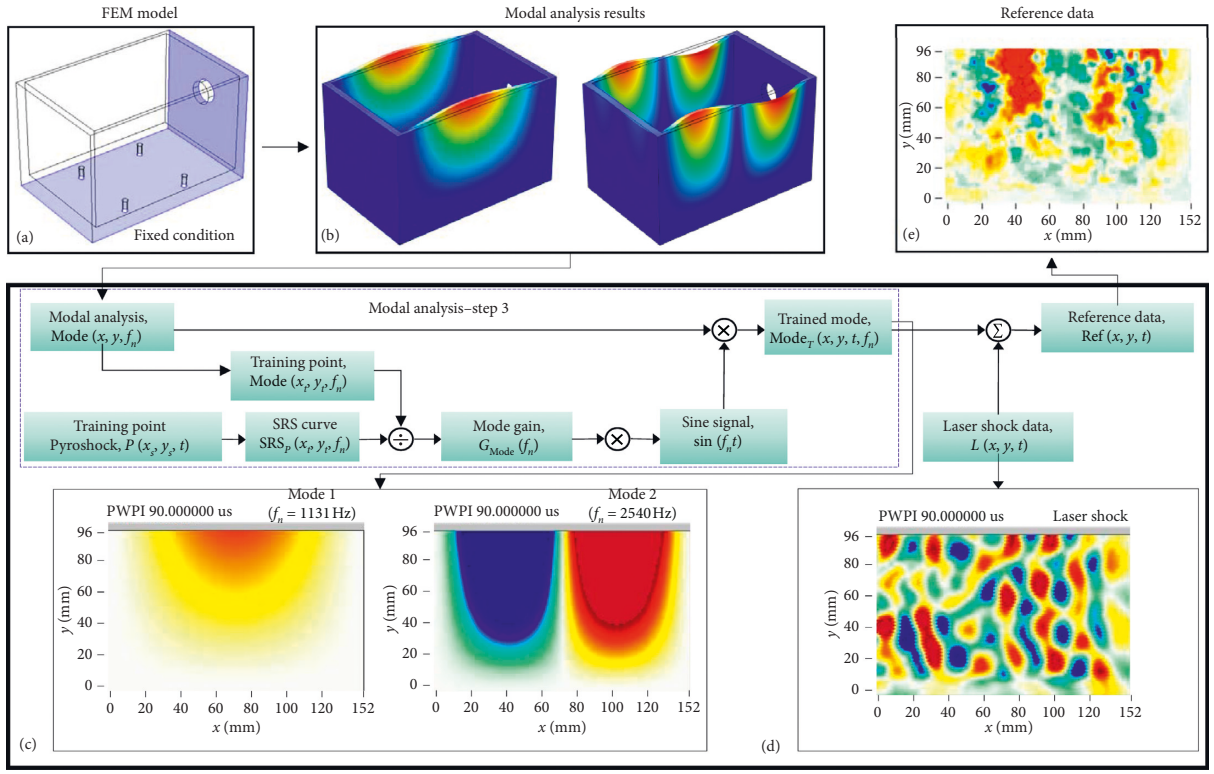

Figure 5: Modal analysis for simulation of pyroshock on the open-box-type tension joint: (a) FEM model, (b) modal analysis results, (c) trained modal analysis data, (d) laser shock data, and (e) reference data.

Figure 4. The data acquisition condition of the laser scanning data is shown in Table 2.

2.3. Modal Analysis for the Simulation of Pyroshock on the Open-Box-Type Tension Joint. Because the PZT sensor used to acquire laser shock scanning data is a contact type and broadband sensor of a central frequency of 200 kHz and a bandwidth of 1.2 MHz, the sensitivity differs, depending on the frequency range. However, the PZT has poor sensitivity in the subkilohertz regime. The pyroshock simulation requires shock signal acquisition over a very wide frequency range, and the laser shock-capturing sensor requires very high sensitivity; however, it is difficult to find such a wide-range PZT sensor covering the whole pyroshock analysis range with high sensitivities over the range. In addition, the LDV is not suitable for the simulation because it provides SNR insufficient for measuring laser shock signal. Therefore, we developed the hybrid method involving the finite element analysis method for the low-frequency pyroshock accompanying vibration and the laser scanning method in the high-frequency regime, utilizing the advantages of each of the two simulation methods. Figure 5 shows the hybrid simulation process. First, modal analysis is performed on the low-frequency vibration regime. Figure 5(a) shows the FEM analysis model and the blue surface means fixed condition. The modal analysis results are shown in Figure 5(b). After completing the modal analysis, Mode (x, y, f_n), expressed by a relative displacement value, is obtained by extracting the result in the interested area. Mode (x_t, y_t, f_n), which is the analysis value at the same point as an arbitrary measurement point of pyroshock, is extracted, and then, the ratio to the $\mathrm{SRS}_P(x_t, y_t, f_n)$ is stored in $G_{\mathrm{Mode}}(f_n)$. $G_{\mathrm{Mode}}(f_n)$ is a representative gain value for all points that convert the modal analysis result saved as the relative displacement value into the amplitude of the actual pyroshock. By multiplying $G_{\mathrm{Mode}}(f_n)$ by Mode (x, y, f_n), the SRS of the pyroshock corresponding to the high-frequency regime is predicted. $\mathrm{Mode}_T(x, y, t, f_n)$ is obtained by providing a sine wave to the predicted SRS of the pyroshock in the low-frequency component as shown in Figure 5(c). Finally, the obtained $\mathrm{Mode}_T(x, y, t, f_n)$ is superimposed with the laser scanning data $L(x, y, t)$ to obtain reference data $\mathrm{Ref}(x, y, t)$ to be used for the pyroshock simulation. Because the open-box-type tension joint used in this experiment was a stainless-steel material, the modal analysis was performed under the

Table 3: Modal analysis condition for pyroshock on the open-box-type tension joint.

FEA software	Young's modulus (GPa)	Density (kg/m^3)	Poisson's ratio	Natural frequency (Hz)	Training point (x_t, y_t)
COMSOL	193	8,000	0.3	1131-first mode 2540-second mode	Point 3–(60, 15)

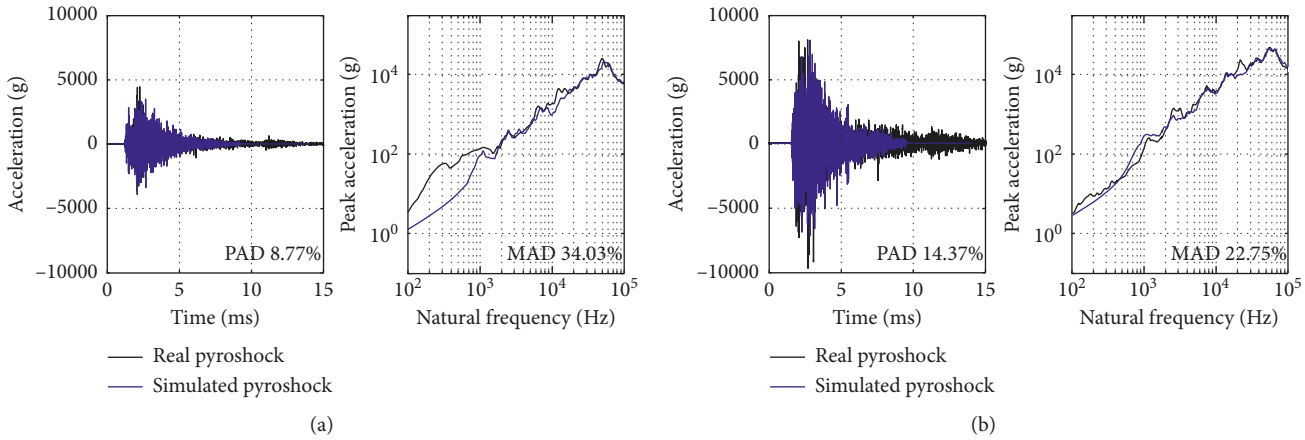

Figure 6: Simulation results of the 1/2-inch explosive bolt-induced shock at training points: (a) Point 1 and (b) Point 3.

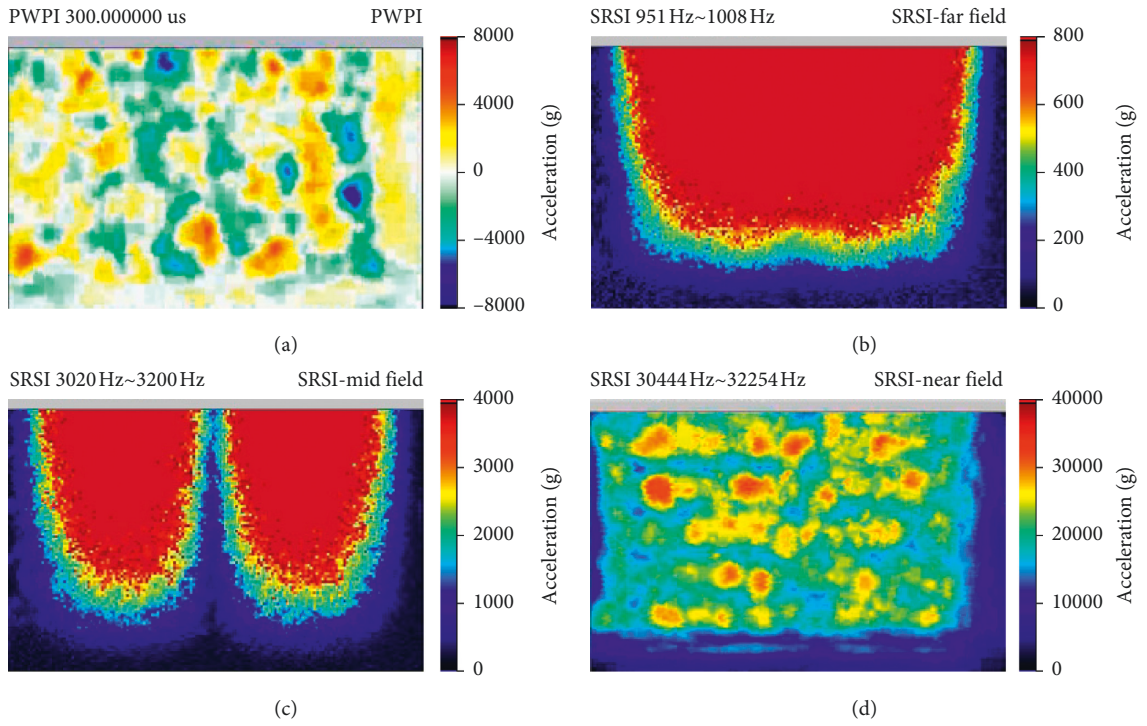

Figure 7: 1/2-inch explosive bolt-induced pyroshock propagation evaluation on the open-box-type tension joint: (a) PWPI at 300 μs, (b) SRSI at 1 kHz, (c) SRSI at 3 kHz, and (d) SRSI at 30 kHz.

conditions shown in Table 3. In the process of obtaining the gain value, pyroshock signals at the measurement point 3 were used.

2.4. 1/2-Inch Explosive Bolt-Induced Shock Simulation on the Open-Box-Type Tension Joint. Using only two sets of pyroshock data, which were measured at point 1 and point 3, a 1/2-inch explosive bolt-induced pyroshock simulation was performed based on iterative signal decomposition and synthesis. Further information on the iterative signal decomposition and synthesis method can be found in reference [14]. Figure 6 shows the pyroshock simulation results at the training point. The black signal represents the actual pyroshock signal, and the blue signal represents the simulation result. At training point 1, the time-

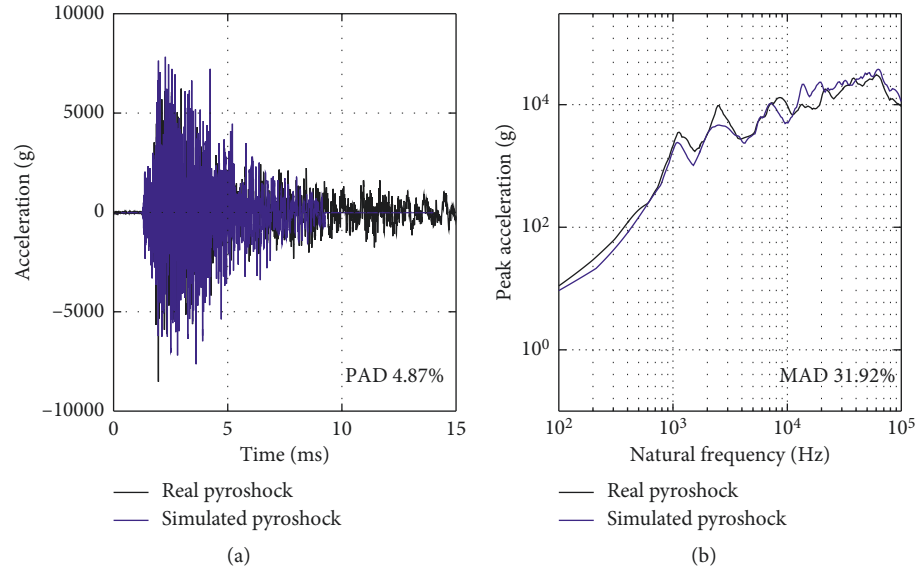

Figure 8: Simulation results of 1/2 inch explosive bolt-induced shock at the verification point.

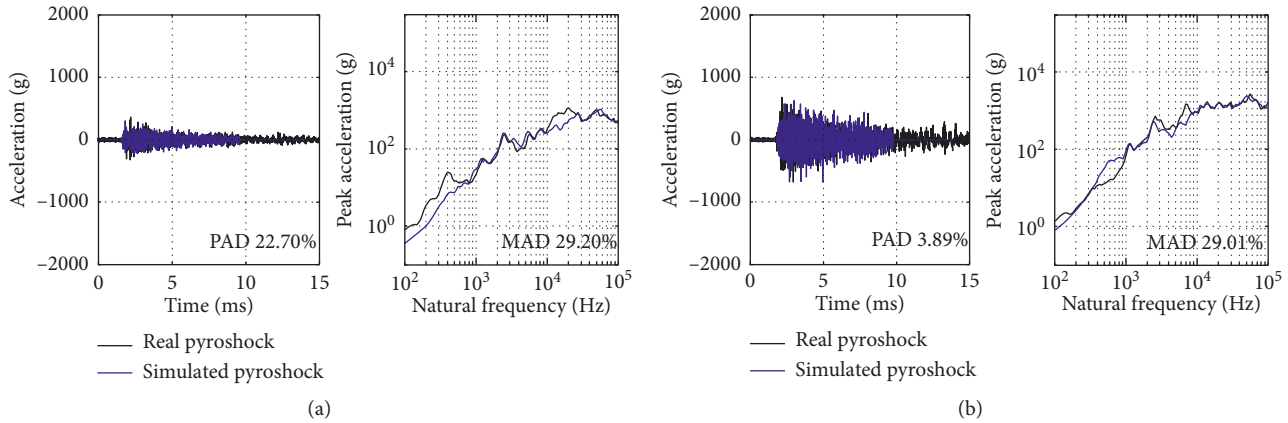

Figure 9: Simulation results of 1/2 inch pyrolock-induced shock at training points: (a) Point 1 and (b) Point 3.

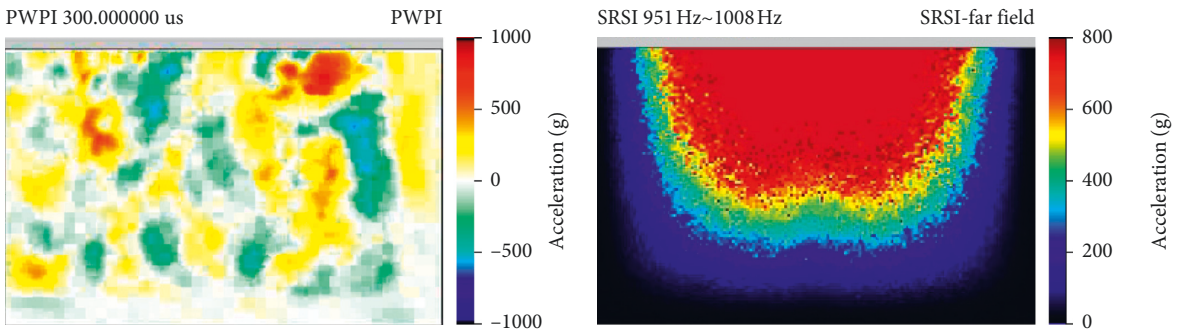

Figure 10: Continued.

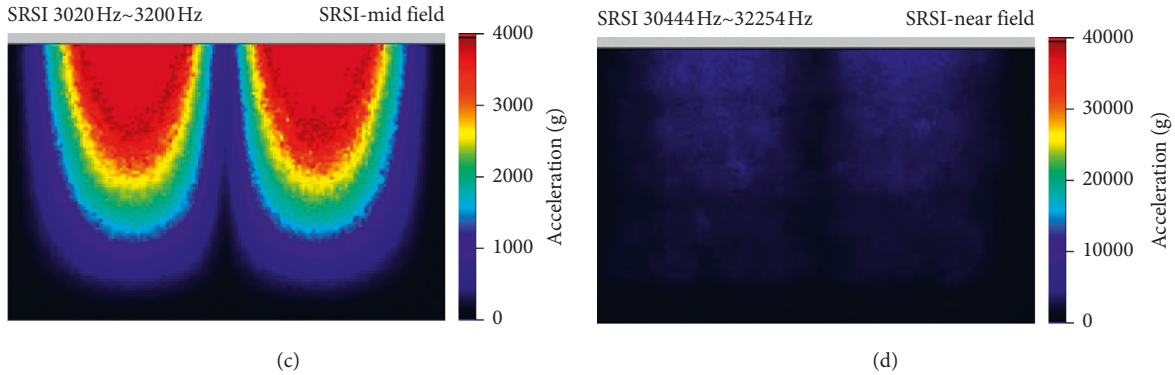

Figure 10: 1/2-inch pyrolock-induced shock propagation evaluation on the open-box-type tension joint: (a) PWPI at 300 μs, (b) SRSI at 1 kHz, (c) SRSI at 3 kHz, and (d) SRSI at 30 kHz.

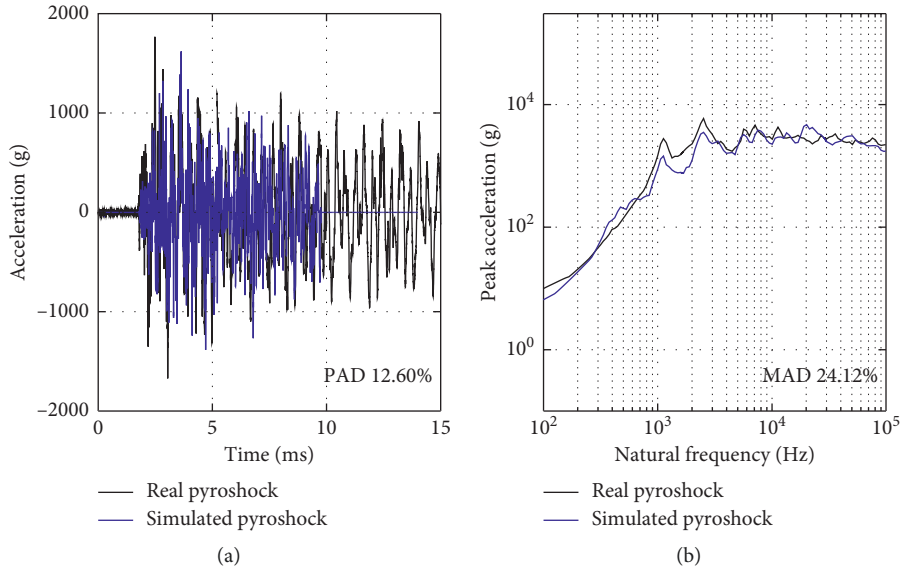

Figure 11: Simulation results of 1/2 inch pyrolock-induced shock at the verification point.

Table 4: Comparison of the peak-to-peak acceleration between the explosive bolt and the pyrolock.

	Peak-to-peak acceleration (g)		
	Point 1	Point 2	Point 3
Explosive bolt	8,158	14,724	17,797
Pyrolock	683	3,393	1,352

domain signal was simulated with a PAD of 8.77%, and the SRS was simulated with an MAD of 34.03%. At training point 3, the time-domain signal was simulated with a PAD of 14.37% and the SRS was simulated with an MAD of 22.75%. The PWPI and SRSI were obtained as shown in Figure 7 by applying the gain value obtained through the training process to all the points equally. Figure 7(a) shows a snapshot of the PWPI at 300 μs, and Figures 7(b)–7(d) show snapshots of the SRSIs at 1 kHz, 3 kHz, and 30 kHz, respectively. To verify the reliability of the obtained PWPI and SRSI, the simulated results were compared with the actual pyroshock at measurement point 2, which was not used at all in the simulation process. As shown in Figure 8, the comparison results confirmed that the time-domain signal was simulated with a PAD of 4.87%, and the SRS was simulated with an MAD of 31.92%.

2.5. 1/2-Inch Pyrolock-Induced Shock Simulation on the Open-Box-Type Tension Joint. Using only two sets of pyroshock data, which were measured at point 1 and point 3, a 1/2-inch explosive bolt-induced pyroshock simulation was performed based on iterative signal decomposition and synthesis. Figure 9 shows the pyroshock simulation results at the

Table 5: Simulation similarity result between the real pyroshock and the simulated pyroshock for each experiment.

	Training point		Verification point	
	$PAD_{average}$ (%)	$MAD_{average}$ (%)	$PAD_{average}$ (%)	$MAD_{average}$ (%)
Explosive bolt	11.57	28.39	4.87	31.92
Pyrolock	13.30	29.11	12.6	24.12

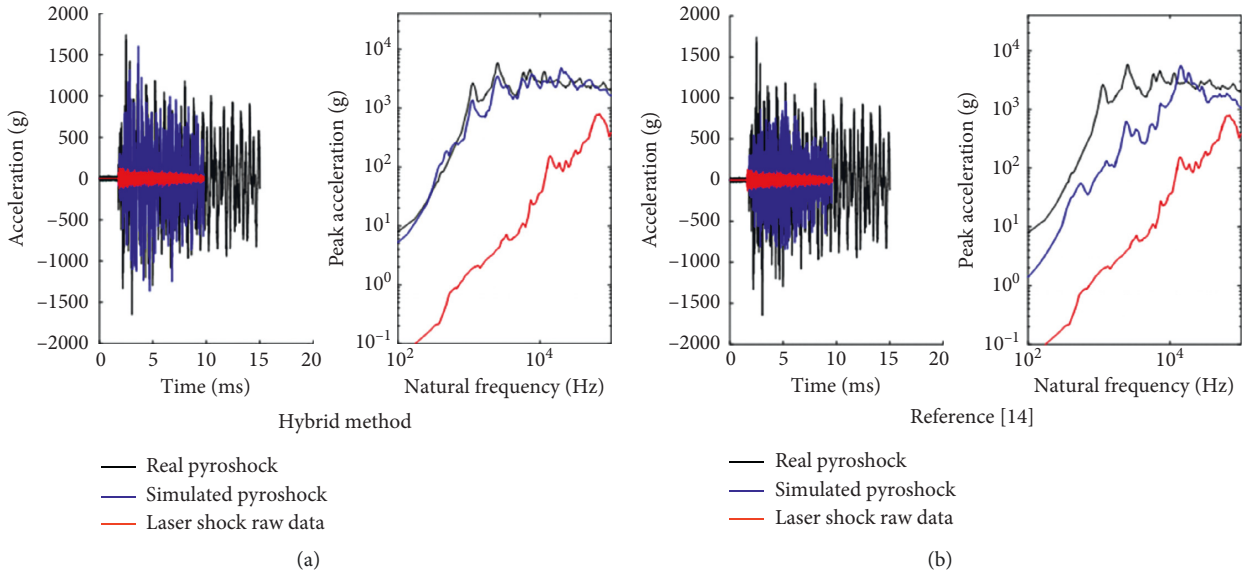

Figure 12: Comparison of the simulation performance between the conventional pyroshock simulation algorithm and the developed algorithm at the verification point: (a) hybrid method and (b) reference [14].

training point. The black signal represents the actual pyroshock signal, and the blue signal represents the simulation result. At training point 1, the time domain signal was simulated with a PAD of 22.70%, and the SRS was simulated with an MAD of 29.20%. At training point 3, the time domain signal was simulated with a PAD of 3.89%, and the SRS was simulated with an MAD of 29.01%. The PWPI and SRSI were obtained as shown in Figure 10 by applying the gain value obtained through the training process to all the points equally. Figure 10(a) shows a snapshot of PWPI at 300 μs, and Figures 10(b)–10(d) show snapshots of SRSI at 1 kHz, 3 kHz, and 30 kHz, respectively. To verify the reliability of the obtained PWPI and SRSI, the simulated results were compared with the actual pyroshock at measurement point 2, which was not used at all in the simulation process. As shown in Figure 11, the comparison results confirmed that the time domain signal was simulated with a PAD of 12.60%, and the SRS was simulated with an MAD of 24.92%.

3. Comparison between Explosive Bolt-Induced Shock and Pyrolock-Induced Shock Using Simulation Results

Table 4 shows the peak-to-peak acceleration of the pyrolock and explosive bolt-induced shocks. The pyrolock-induced shock compared to the explosive bolt shows the impulse amount of 1/12 level at measurement points 1 and 3 and 1/5 level at measurement point 2. Because the pyroshock is affected by the geometrical shape of the structure, the impulse ratio of the two pyrodevices differs depending on the measurement point. Therefore, it is difficult to quantitatively evaluate the impulse of pyrolock and explosive bolt based on only the peak-to-peak acceleration information at three points. The system developed in this study simulated pyroshock at all points and visualized the pyroshock in the time domain and frequency domain to quantitatively compare the impulse amount of an explosive bolt and a pyrolock. Before comparing the simulation results, we first summarize the similarity between the actual pyroshock and simulation results in Table 5 to verify the simulation results. The time-domain signal was simulated with an averaged PAD of 11.2%, and the SRS was simulated with an averaged MAD of 28.5%. Figure 12 shows that the simulation performance is improved compared to the pyroshock simulation method based on the laser shock developed in the past. Moreover, considering that the repeatability of the pyroshock itself is approximately 20% [14], the simulation performance is satisfactory. Because the reliability of the simulation results was verified, the impulses of an explosive bolt and a pyrolock were analyzed using the simulation results. Figure 13(a) shows the result of

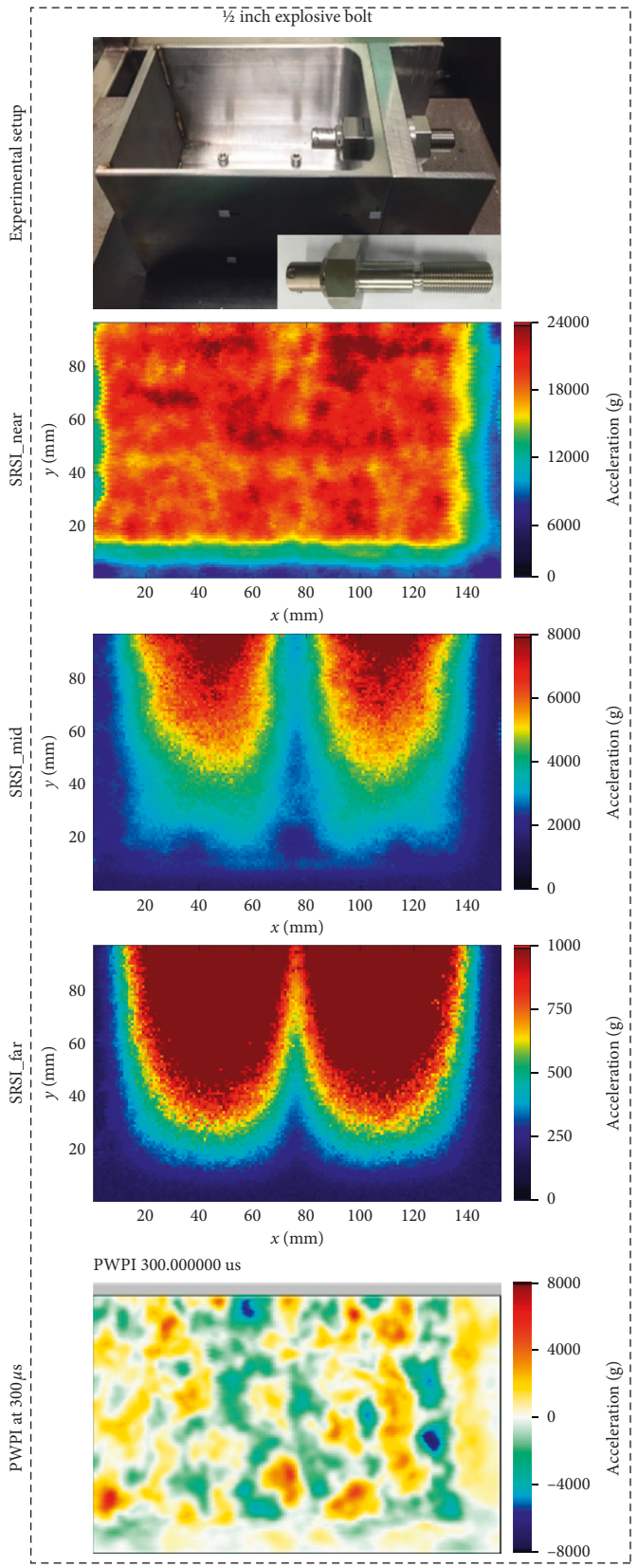

(a)

Figure 13: Continued.

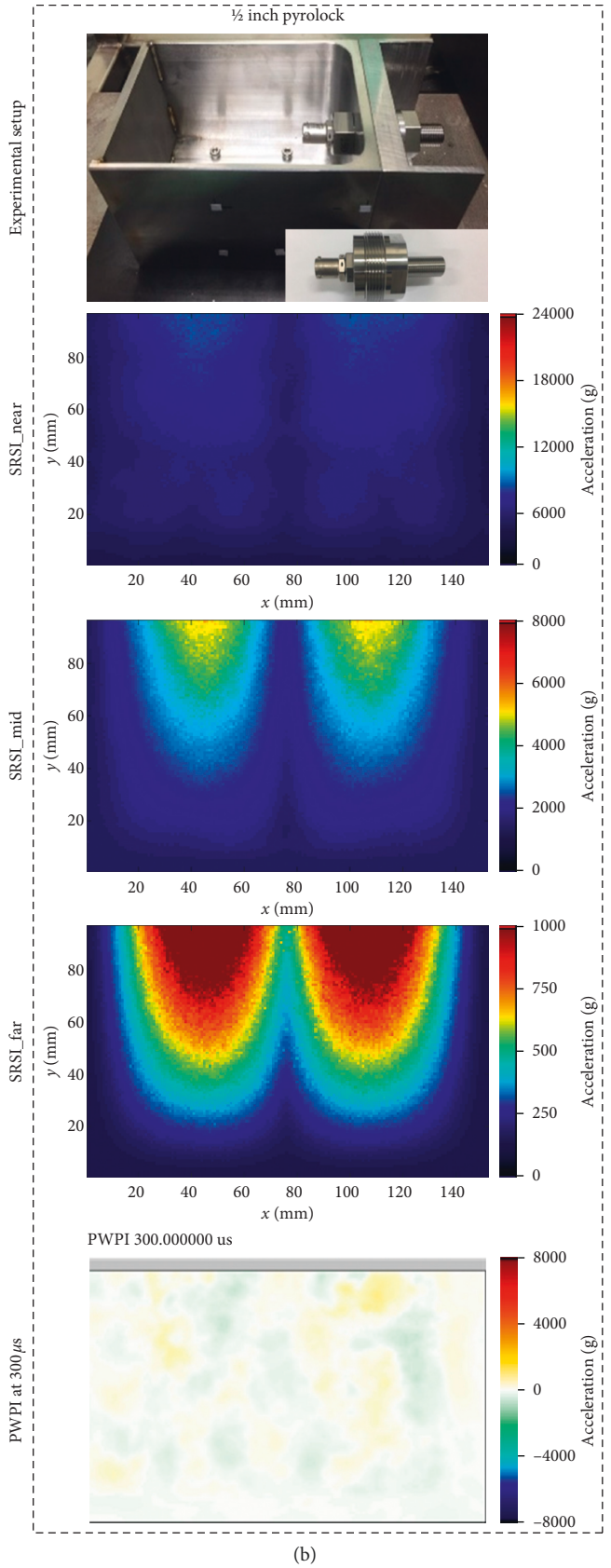

Figure 13: Evaluation of the pyroshock propagation in temporal and spectral domains on the open-box-type specimen: (a) simulation results of 1/2 inch explosive bolt-induced pyroshock (b) simulation results of 1/2 inch pyrolock-induced pyroshock.

visualization of the explosive bolt-induced shock in the time domain and frequency domain, and Figure 13(b) shows the visualization of the pyrolock-induced shock in the time domain and frequency domain. Comparing the simulation results in the time domain using the PWPI, the pyrolock is found to have a smaller impulse amount compared to the conventional explosive bolt. Because the time-domain signal is a superposition of various frequency components, it is necessary to confirm which frequency component is reduced. The SRSI is divided into a far-field regime corresponding to 100 Hz to 3 kHz including a low-frequency vibration component, a mid-field regime corresponding to 3 kHz to 10 kHz, and a near-field regime corresponding to 10 kHz to 100 kHz. In the far field, the two shocks do not show a large difference, whereas in the mid-field and near-field regime, a marked decrease in the amount of pyrolock impulse is found.

4. Conclusions

In this study, we developed a hybrid method of modal analysis and laser shock scanning to visualize the pyroshock propagation accompanying vibration according to the boundary condition and to evaluate the risk of pyroshock. The hybrid method predicts the characteristics of pyroshock in the open-box tension joint by combining laser shock and modal analysis where the modal analysis was used to superimpose the low-frequency vibration to pyroshock propagation; Both laser shock and modal analysis results were superposed and reconstructed to the pyroshock using iterative signal decomposition and synthesis. The pyroshock propagation characteristics of the two different pyrodevices, an explosive bolt and a pyrolock, in the open-box-type tension joint were simulated using the developed hybrid simulation method. The time-domain signal was simulated with an averaged PAD of 11.2%, and the SRS was simulated with an averaged MAD of 28.5%. Considering that the repeatability of the pyroshock itself is approximately 20%, the simulation performance was found to be satisfactory. On the contrary, simulation results at point 1 show relatively higher MAD and PAD than the other two points. The reason was that the point 1 showed much more complex response than the other two points since it was the result of measurement near the stiffer boundary. In order to improve the simulation results in this boundary, further investigation of various wave modes seems necessary. We visualized the simulation results in the temporal and spectral domains to compare the pyroshock induced by each pyrodevice. A comparison of the simulations showed that the pyrolock has an impulse level 1/12 in magnitude compared to that of the explosion bolt. In particular, it was confirmed that, in the near field, the pyrolock-induced shock has a smaller impulse magnitude than the explosive bolt-induced shock. The hybrid method developed in this paper demonstrated that it is possible to simulate pyroshock over the entire frequency regime in complex specimens accompanying vibration and to evaluate the risk in time and frequency domains.

Data Availability

The data used to support the findings of this study are available from the corresponding author upon request.

Conflicts of Interest

The authors declare that there are no conflicts of interest regarding the publication of this paper.

Acknowledgments

This research was supported by the National Research Foundation of Korea (NRF) Grant funded by the Ministry of Science and ICT (NRF-2017R1A5A1015311) and by the research grant (PMD) of the Agency for Defense Development and Defense Acquisition Program Administration of the Korean government.

References

[1] L. J. Bement, "Pyrotechnic system failures: causes and prevention," in *NASA Technical Memorandum 100633*, pp. 1–3, NASA, Washington, DC, USA, 1988.

[2] E. Fillippi, H. Attouoman, and C. Conti, "Pyroshock simulation using the alcatel etca test facility, in: launch vehicle vibrations," in *Proceedings of the 1st European Conference*, pp. 1–3, CNES, Toulouse, France, June 1999.

[3] L. J. Bement and M. L. Schimmel, "A manual for pyrotechnic design, development and qualification," in *NASA Technical Memorandum*, vol. 110–172, p. 3, NASA, Washington, DC, USA, 1995.

[4] C. J. Moening, "Pyrotechnic shock flight failures," in *Proceedings of the Institute of Environmental Sciences Pryotechnic Shock Tutorial Program, 31st Annual Technical, Meeting*, pp. 2–4, Washington, DC, USA, May 1985.

[5] IEST-RP-DTE032.2, *Pyroshock Testing Techniques*, Institute of Environmental Sciences and Technology, Schaumburg, IL, USA, 2011.

[6] MIL-STD-810F, *Environmental Engineering Considerations and Laboratory Tests*, Department of Defense, USA, Pentagon, VA, USA, 2000.

[7] Anon, "Pyroshock test criteria," in *NASA Technical Standard NASA-STD 7003A*, p. 15, NASA, Washington, DC, USA, 2011.

[8] J. E. Alexander, "Shock response spectrum a primer," *Sound and Vibration*, vol. 43, pp. 6–14, 2009.

[9] T. Irvine, *An Introduction to the Shock Response Spectrum*, Arizona State University, Tempe, AZ, USA, 2002.

[10] N. T. Davie and V. I. Bateman, "Pyroshock simulation for satellite components using a tunable resonant fixture—phase 2," Sandia report SAND93- 2294, pp. 5–12, Sandia National Labs, Albuquerque, NM, USA, 1997.

[11] T. J. Dwyer and D. S. Moul, "Pyro shock simulation: experience with the MIPS simulator," in *Proceedings of the Space Simulation Conference: Support the Highway to Space Through Testing*, pp. 125–138, Williamsburg, VA, USA, 1988.

[12] Y. J. Mao, H. J. Huang, and Y. X. Yan, "Numerical techniques for predicting pyroshock responses of aerospace structures," *Advanced Materials Research*, vol. 108–111, pp. 1043–1048, 2010.

[13] A. R. Kolaini and J. P. Fernandez, "Qualifying flight hardware for pyroshock environments: shock simulation systems and modeling," in *Proceedings of the Workshop on Spacecraft*

Shock Environment and Verification, p. 20, Noordwijk, Netherlands, 2015.

[14] Y.-W. Kim, J.-K. Jang, and J.-R. Lee, "Pyroshock simulation algorithm in temporal and spectral domains based on laser shock scanning and iterative decomposition and synthesis considering stop band effects," *Shock and Vibration*, vol. 2017, Article ID 8351791, 19 pages, 2017.

[15] B.-H. Jung, Y.-W. Kim, J.-R. Lee, and D. S. Kim, "Visualization of pyroshock wave reduction by insulator using a laser shock based simulation method," *Measurement*, vol. 137, pp. 302–311, 2019.

[16] Y. Choi and J.-R. Lee, "Multi-directional adjacent wave subtraction and shifted time point mapping algorithms and their application to defect visualization in a space tank liner," *NDT & E International*, vol. 86, pp. 53–64, 2017.

[17] J. Lee, J.-H. Han, Y. Lee, and H. Lee, "A parametric study of ridge-cut explosive bolts using hydrocodes," *International Journal of Aeronautical and Space Sciences*, vol. 16, no. 1, pp. 50–63, 2015.

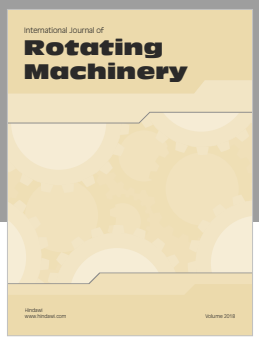

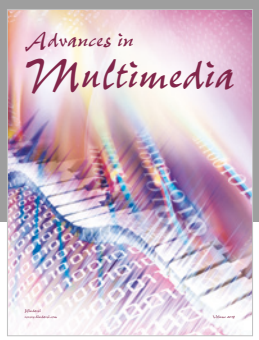

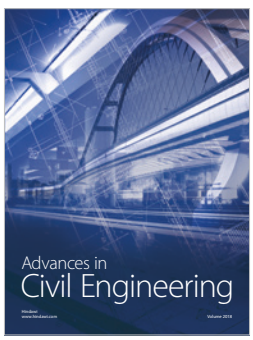

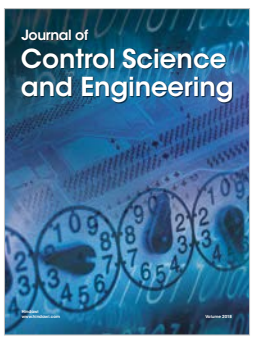

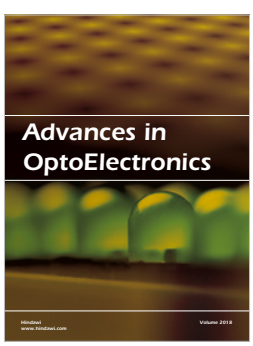

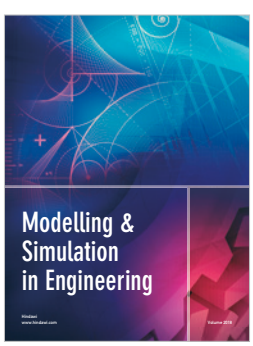

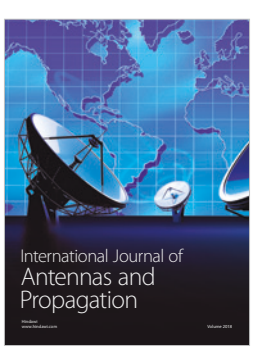

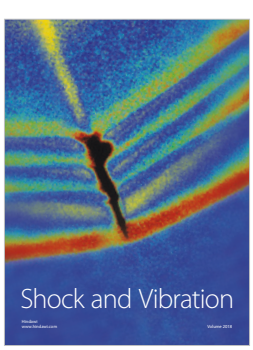

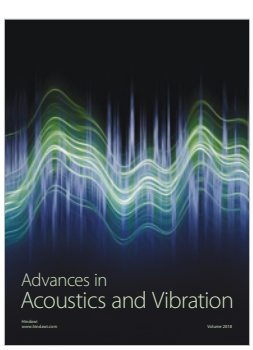

Hindawi

Submit your manuscripts at
www.hindawi.com